Application of Hydrodechlorination in Environmental Pollution Control: Comparison of the Performance of Supported and Unsupported Pd and Ni Catalysts

Claudia AMORIM[a], Xiaodong WANG, Mark A. KEANE[*]

Chemical Engineering, School of Engineering and Physical Sciences, Heriot-Watt University,
Edinburgh EH14 4AS, Scotland, United Kingdom

Abstract: Catalytic hydrodechlorination (HDC) is an innovative means of transforming chlorinated waste streams into a recyclable product. In this study, the gas phase HDC of chlorobenzene (CB) has been studied over bulk Pd and Ni and ((8 ± 1) wt%) Pd and Ni supported on activated carbon (AC), graphite, graphitic nanofibers (GNF), Al_2O_3, and SiO_2. Catalyst activation was examined by temperature-programmed reduction (TPR) analysis and the activated catalysts characterized in terms of BET area, transmission electron microscopy, scanning electron microscopy, H_2 chemisorption/temperature-programmed desorption, and X-ray diffraction measurements. Metal surface area (1–19 m^2/g), TPR, and H_2 uptake/release exhibited a dependence on both metal and support. The Pd system delivered specific HDC rates that were up to three orders of magnitude greater than that recorded for the Ni catalysts, a result that we link to the higher H_2 diffusivity in Pd. HDC was 100% selective over Ni while Pd also produced cyclohexane (selectivity < 4%) as a result of a combined HDC/hydrogenation. Bulk Pd outperformed carbon supported Pd but was less active than Pd on the oxide supports. In contrast, unsupported Ni presented no measurable activity when compared with supported Ni. The specific HDC rate was found to increase with decreasing metal surface area where spillover hydrogen served to enhance HDC performance.

Key words: hydrodechlorination; chlorobenzene; bulk palladium and nickel catalysts; activated carbon; graphite; carbon nanofiber; alumina; silica; spillover hydrogen

CLC number: O643   **Document code:** A

Halogen containing waste is typically xenobiotic and, having no analogous compounds in nature, there is no natural means of ameliorating the negative environmental impact. The presence of organo-halogens in effluent discharges is of increasing concern due to the mounting evidence of adverse stratospheric ozone, ecological, and public health impacts [1,2]. The legislation imposed by regulatory bodies is certain to become increasingly more restrictive. This has leant an added degree of urgency to the development of effective control strategies. In addition to the legislative demands, the economic pressures faced by the commercial sector in the 21st century include loss of potentially valuable resources through waste, escalating disposal charges and increasing raw material/energy costs. Chloro-aromatics, the focus of this study, are commercially important chemicals, used as end products and intermediates in the manufacture of plastics, dyes, a diversity of agrochemicals, and as heat transfer media [3,4]. Catalytic hy-

drodechlorination (HDC) is now recognized as a non-destructive low energy methodology for the transformation of toxic chlorinated streams into valuable raw material with no directly associated NO_x/SO_x emissions or dioxin/furan formation [3,5]. In this study, we have adopted the HDC of chlorobenzene (CB) as a model reaction to probe support effects for reaction over Pd and Ni catalysts.

Catalytic CB HDC has been investigated using an array of supported metals, notably Pd [6–15], Pt [7,8,16], Ni [7–9,16–25], Rh [8,16], and Ru [16,26] where the supports that have been used include carbon [7,19–21,26], ZrO_2 [6], Al_2O_3 [7,11,19–21,24], SiO_2 [12,13,18–22,24], MgO [15,19–21,24], Nb_2O_5 [14], TiO_2 [10,24], zeolite [24], and AlF_3 [7]. The primary function of the catalyst support is to provide a surface on which the metal is dispersed in order to obtain smaller metal particle sizes and, consequently, higher metal surface areas which, in turn, can favorably impact on catalytic activity. Moreover, product selectivity and catalyst

stability can also be influenced by the nature of the catalyst support [3]. Such factors as metal-support interaction, porosity, and acid-base properties have been considered to a limited extent in catalytic dehalogenation applications [3,8,19,27]. It should be noted that the studies cited above did not consider the HDC response of the corresponding unsupported metal, which is an essential test of the influence of the support on intrinsic catalytic activity. Wu and Xu [28] have, however, compared the action of Raney Ni with Ni/AC, Ni/Al$_2$O$_3$, and Ni/SiO$_2$ in the liquid phase HDC of CB (at 1 MPa H$_2$) and found that Raney Ni outperformed Ni/Al$_2$O$_3$ and Ni/SiO$_2$ but was less active than Ni/AC.

Unsupported mono- and bi-metallic catalysts such as Pd [29–31], Ni [32–34], Pd/Fe [35], Pd/Zn [35], Pt/Fe [35], and Ni/Fe [35] have been used to promote the dehalogenation of chlorofluorocarbon (CFC) [30,31,33], dichlorotetrafluoroethane [29,31], chloroethenes [35], vinyl chloride [35], dichlorobenzene [34], trichlorobenzene [32], and chloro-organic mixtures [35]. While it may be expected that a well dispersed supported metal catalyst should exhibit higher specific activity than the bulk metal, there are examples in the literature [30,33,36] of unsupported systems that deliver similar or greater dehalogenation rates when compared with corresponding supported catalyst(s). The properties of a catalyst support critical to achieving optimum HDC performance have yet to be conclusively established. In this paper, we compare the action of supported and unsupported Pd and Ni in the gas phase HDC of CB, linking the catalytic response to pertinent catalyst characterization measurements. Five different supports, three carbon-based and two oxides, have been considered: (1) conventional activated carbon (AC); (2) graphite; (3) graphitic nanofibers (GNF); (4) Al$_2$O$_3$; (5) SiO$_2$. Application of Pd/GNF and Pd/graphite in CB HDC was first reported in our previous work [37] and a search through the literature failed to unearth any reports of Ni/GNF use as catalyst in HDC processes. Additionally, to the best of our knowledge, this is the first reported direct comparison of gas phase CB HDC over unsupported Pd and Ni and the corresponding oxide/carbon supported catalysts.

1   Experimental

1.1   Catalyst preparation and activation

The AC (G-60, 100 mesh) support was obtained from NORIT (UK), the graphite (synthetic 1–2 μm powder), and SiO$_2$ (fumed) were supplied by Sigma-Aldrich and the Al$_2$O$_3$ support (Puralox) was provided by Condea Vista Co. The GNF support was synthesized by the catalytic decomposition of ethylene, as described in detail previously [27,38], contacted with 1 mol/L HNO$_3$ to remove any residual metal particles and subjected to a partial oxidation (in

5% v/v O$_2$/He) at 673 K for 2 h to remove the amorphous carbon content. The commercial AC and graphite samples were also subjected to the same demineralization; the carbon supports were thoroughly washed with deionized water (until pH approached 7) and oven-dried at 383 K for 12 h. The supported Pd and Ni catalysts ((8 ± 1) wt%) were prepared by standard impregnation where a 2-butanolic Pd(NO$_3$)$_2$ or Ni(NO$_3$)$_2$ solution was added drop wise at 353 K to the substrate with constant agitation (600 r/min) and oven dried at 393 K for 16 h. The metal loading (reproducible to within ± 4%) was determined by inductively coupled plasma-optical emission spectrometry (ICP-OES, Vista-PRO, Varian Inc.). Prior to use in catalysis, the precursors, sieved (ATM fine test sieves) into a batch of 75 μm average particle diameter, were reduced directly in a 60 cm^3/min stream of ultra-pure dry H$_2$ at 10 K/min to (523 ± 1) K (Pd system) or (723 ± 1) K (Ni system), which was maintained for at least 12 h. PdO (99.998%) and NiO (99%), the unsupported Pd and Ni catalyst precursors, respectively, were obtained from Sigma-Aldrich and activated as above.

1.2   Catalyst characterization

BET surface area, temperature-programmed reduction (TPR), H$_2$ chemisorption and temperature-programmed desorption (TPD) analyses were conducted on the bulk metals and supported catalysts using the commercial CHEMBET 3000 (Quantachrome Instrument) unit, employing a thermal conductivity detector (TCD) where a known mass (≤ 0.1 g) of sample was loaded into a U-tube (10 cm × 3.76 mm i.d.): data acquisition/manipulation employed the TPR Win^{TM} software. BET areas were recorded in a 30% v/v N$_2$/He flow; pure N$_2$ (99.9%) served as the internal standard. At least two cycles of N$_2$ adsorption-desorption were employed to determine total surface area using the standard single point method. TPR employed a reducing gas mixture of 5% v/v H$_2$/N$_2$ (mass flow controlled at 20 cm^3/min) with a heating rate of 10 K/min to 523 K (for Pd catalysts) or 723 K (for Ni catalysts); the effluent gas was directed through a liquid N$_2$ trap. The reduced samples were swept with a flow of N$_2$ for 1 h, cooled to room temperature, and subjected to H$_2$ chemisorption using a pulse (50 μl) titration procedure. At this pulse volume, the maximum partial pressure of H$_2$ in the sample cell (0.004 atm) was well below 0.013 atm, the pressure needed for Pd hydride formation at room temperature [39]. Hydrogen pulse introduction was repeated until the signal area was constant, indicating surface saturation. The specific metal surface area (S, m^2/g) of the supported catalysts was calculated from H$_2$ chemisorption assuming an adsorption stoichiometry of H:Me = 1:1 (Me = Pd or Ni). The samples were then thoroughly flushed with N$_2$ for 30 min and TPD

was conducted in N_2 at 50 K/min to 873 K. Based on TCD calibrations and analysis of the effluent gas using a MICROMASS PC Residual Gas Analyzer, the TPD profiles recorded in this paper can be attributed solely to H_2 release. BET surface area and H_2 uptake values were reproducible to within ± 3% and the values quoted in this paper are the mean. Powder X-ray diffraction (XRD) patterns were recorded with a Philips X'Pert instrument using Ni filtered Cu K_α radiation. The samples were mounted in a low background sample holder and scanned at a rate of 0.02º/s over the range $20º \leq 2\theta \leq 90°$. The diffraction patterns were compared with the JCPDS-ICDD [40] reference data for identification purposes. Analysis by scanning electron microscopy (SEM) was carried out using a Hitachi S900 field emission SEM, operated at an accelerating voltage of 25 kV; the sample was deposited on a standard aluminum SEM holder and coated with gold. The transmission electron microscopy (TEM) analyses were conducted using a JEOL 2000 TEM microscope operated at an accelerating voltage of 200 kV. The catalyst sample was dispersed in 1-butanol by ultrasonic vibration, deposited on a lacey-carbon/Cu grid (200 Mesh), and dried at 383 K for 12 h before TEM analysis.

1.3 Catalysis procedure

Reactions were carried out under atmospheric pressure in a fixed-bed glass reactor (i.d. = 15 mm) with a co-current flow of CB in H_2 at 423 K (for Pd catalysts) or 473 K (for Ni catalysts). The catalytic reactor, and operating conditions/criteria employed to ensure negligible heat/mass transport limitations, have been described in detail elsewhere [41,42] but some features, pertinent to this study, are given below. CB HDC was performed at inlet Cl to metal ratios of 3.1×10^2–6.1×10^3 $mol_{Cl}/(mol_{Pd}·h)$ and 90 $mol_{Cl}/(mol_{Ni}·h)$ where the GHSV was maintained at 2×10^4 h^{-1}. The CB reactant was fed by means of a microprocessor controlled infusion pump (Model 100, kd Scientific) via a glass/teflon air tight syringe and a teflon line to the reactor in a stream of ultra pure H_2, the flow rate of which was monitored using a Humonics 520 digital flow meter. The reaction products were analyzed by capillary GC as described previously [42]. The relative peak area % was converted to mol% using regression equations based on detailed calibration and the detection limit corresponded to a feedstock conversion < 0.4 mol%: overall analytic reproducibility was better than ± 3%. Repeated catalytic runs with different samples from the same batch of catalyst delivered product compositions that were reproducible to within ± 7%. As blank tests, passage of CB in a stream of H_2 through the empty reactor or over the supports alone, i.e. in the absence of Pd or Ni, did not result in any detectable conversion. The CB reactant was used as received (Sigma-Aldrich, 99.9%) and ultra high purity (99.999%) H_2, He, and N_2 were supplied by Scott-Gross Co. Inc.

2 Results and discussion

2.1 Catalyst characterization

Metal loading (supported catalysts), BET surface area, H_2 uptake, and specific metal surface areas (S) are given in Table 1. The AC support is characterized by a large surface area with significant micro-/meso-porosity (average pore radius = 3.2 nm); pore volume = 0.5 cm^3/g. Graphite has limited porosity (pore volume < 0.05 cm^3/g) with a low associated surface area. The high aspect (length to diameter) ratio and fibrous nature of the GNF support is immediately apparent from the SEM shown in Fig. 1(a). High resolution TEM analysis, presented elsewhere [43], has demonstrated that the GNF support is characterized by a "ribbon" structure where the graphene layers are oriented parallel to the fiber axis. A representative TEM image presented in Fig. 1(b) illustrates the nature of the Pd particle morphology and dispersion on the GNF support. The interest in GNF as a catalyst support has increased in the last decade with applications in hydrogenation [43–46], ammonia synthesis [47], selective oxidation [48], and hydrazine decomposition [49]. This is due, in part, to the lower associated mass transfer constraints when compared with AC [44,48]. Moreover, AC exhibits variable structural characteristics when produced from different sources [49] while there is greater control over GNF structure during synthesis [44]. BET surface areas of the Al_2O_3 and SiO_2 based catalysts are similar and are in agreement with values quoted in the literature [50,51].

Table 1 Metal loading, BET area, volume of H_2 chemisorbed, and specific metal surface areas (S) associated with the activated Pd and Ni catalysts

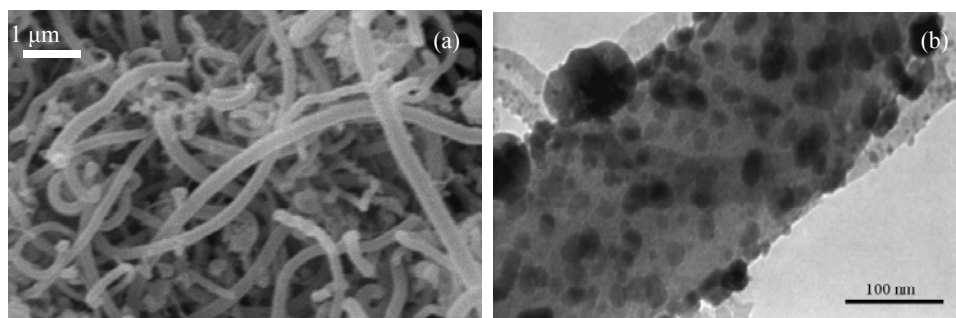| Catalyst	Metal loading (wt%)	BET surface area (m^2/g)	H_2 uptake (cm^3/g)	S (m^2/g)
Pd	—	2	0.3	2.0
Pd/AC	7.8	875	1.0	3.8
Pd/graphite	8.5	11	2.2	8.7
Pd/GNF	8.7	86	1.7	6.7
Pd/Al_2O_3	8.2	173	1.8	7.1
Pd/SiO_2	8.3	180	3.7	14.4
Ni	—	4	<0.02	1.0
Ni/AC	8.5	852	3.8	12.1
Ni/graphite	7.0	9	0.4	1.3
Ni/GNF	7.5	92	2.0	6.5
Ni/Al_2O_3	7.7	154	4.5	14.4
Ni/SiO_2	8.4	183	5.9	18.8

Fig. 1. SEM image of the GNF support (a) and TEM image of the supported Pd phase in Pd/GNF (b).

The XRD patterns for the activated samples, given in Fig. 2, show no evidence of any bulk PdO or NiO. The four peaks that characterize the Pd samples (see Fig. 2(a)) at 2θ = 40.1°, 46.7°, 68.1°, and 82.15° correspond, respectively, to Pd(111), (200), (220), and (311) planes and are consistent with an exclusive cubic symmetry. The diffractograms generated for the Ni samples (Fig. 2(b)) exhibit three peaks (at 44.5°, 51.8°, and 76.3°, corresponding to (111), (200), and (220) planes of metallic nickel), also characteristic of cubic symmetry. The markers included in Fig. 2 illustrate the position and relative intensity of the XRD peaks for cubic Pd and Ni, taken from the JCPDS standards [40]. The XRD patterns for Pd/graphite and Ni/graphite are dominated by a peak at 2θ = 26° that is characteristic of structured (graphitic) carbon. While the XRD signals for Pd/GNF and Ni/GNF also demonstrate the strong presence of a graphitic phase, the broadness of the 2θ = 26° peak is indicative of a lesser long range structural order.

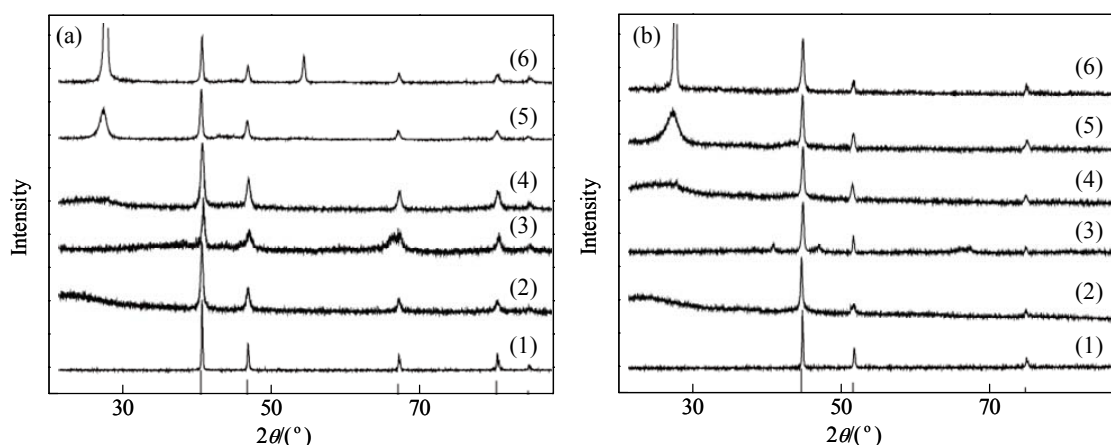**Fig. 2.** XRD patterns for the reduced/passivated catalyst samples. (a) Pd (1), Pd/SiO$_2$ (2), Pd/Al$_2$O$_3$ (3), Pd/AC (4), Pd/GNF (5), Pd/graphite (6); (b) Ni (1), Ni/SiO$_2$ (2), Ni/Al$_2$O$_3$ (3), Ni/AC (4), Ni/GNF (5), Ni/graphite (6). Note: the solid lines indicate peak position (with relative intensity) for cubic Pd (a) and Ni (b).

The TPR profiles generated for all the Pd and Ni catalysts are given in Fig. 3. The level of reproducibility of the TPR response can be assessed from the repeated TPR measurements included in Fig. 3. The TPR profiles associated with the unsupported Pd and the three carbon supported Pd are characterized by a single negative peak, i.e. H$_2$ production. The occurrence of a negative TPR peak has been observed previously and attributed to H$_2$ release due to the decomposition of β-phase Pd hydride [12,36,52]. It is well established that Pd can adsorb H$_2$ at room temperature to form a hydride [39,52] where the H$_2$ partial pressure exceeds 0.013 atm [39]. In contrast to Pd, the formation of Ni hydride at room temperature via contact with H$_2$ gas is very demanding, requiring H$_2$ pressures in excess of 3000 atm [53]. The temperature corresponding to maximum H$_2$ release/hydride decomposition for unsupported Pd (ca. 386 K) is higher than that (368–377 K) recorded for the supported catalysts. Palladium hydride decomposition from supported Pd has been reported in the literature to occur over the range 323–373 K [12,36,52–54]. Moreover, the decomposition temperature has been proposed to increase with increasing H$_2$ partial pressure and Pd particle size [52]. The latter response is consistent with our observation that a higher temperature is required for bulk Pd hydride decomposition compared with the supported systems. The absence of any detectable H$_2$ consumption (during TPR) in advance of H$_2$ release suggests a room temperature reduction, prior to TPR. Indeed, there is a general agreement in the literature
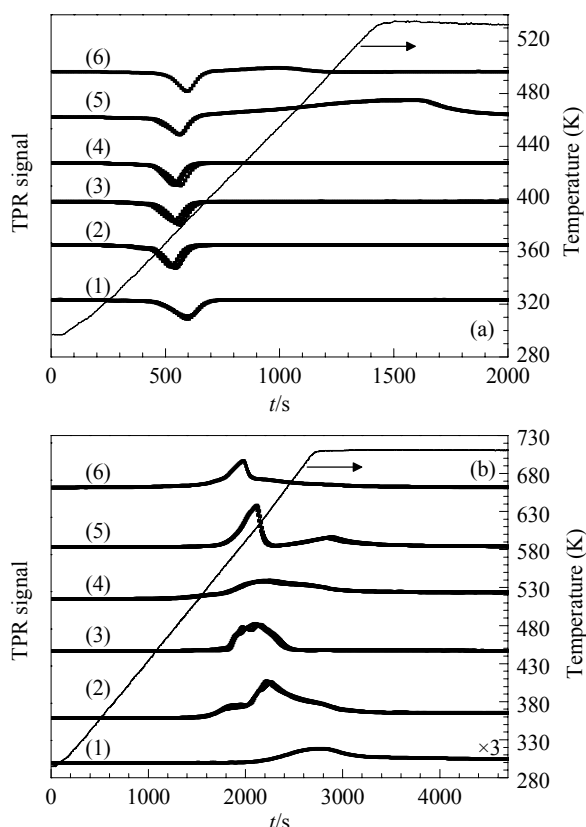
Fig. 3. TPR profiles of different catalyst samples. (a) PdO (1), Pd/AC (2), Pd/graphite (3), Pd/GNF (4), Pd/Al$_2$O$_3$ (5), Pd/SiO$_2$ (6); (b) NiO (1), Ni/AC (2), Ni/graphite (3), Ni/GNF (4), Ni/Al$_2$O$_3$ (5), Ni/SiO$_2$ (6).

that the reduction of supported and unsupported PdO occurs at room temperature [55,56]. In addition to H$_2$ release/hydride decomposition, the TPR profiles for Pd/Al$_2$O$_3$ and Pd/SiO$_2$ also included ill-defined positive peaks (H$_2$ consumption) during the temperature ramp that extended into the final isothermal hold in the case of Pd/Al$_2$O$_3$, suggesting an oxide support effect that serves to stabilize the Pd precursor, requiring a higher reduction temperature. This is in line with previous reports wherein H$_2$ consumption peaks up to 523 K were recorded for the TPR of PdO supported on Al$_2$O$_3$ and SiO$_2$ [57,58].

In contrast to the Pd system, the TPR profiles (Fig. 3(b)) of the Ni catalysts presented only positive peaks with a H$_2$ consumption during the temperature ramp; the associated T_{max} values span the range 598–709 K. A two stage reduction has been proposed elsewhere [59] for the direct (without pre-calcination) TPR of a supported nickel nitrate precursor where thermal decomposition of the nitrate to NiO precedes the subsequent reduction of NiO to Ni^0. TPR T_{max} values at 630 K [60], 651 K [61], and 723 K [62] have been attributed to a reduction of NiO on SiO$_2$. González-Marcos

and co-workers [63] linked their single TPR peak at 601 K directly to Ni(NO$_3$)$_2$ decomposition. The TPR profile generated in this study for bulk NiO yielded a single broad peak (573–723 K) that is in good agreement with the measurements provided by Roh et al. [64] and matches the higher temperature region of H$_2$ consumption associated with the supported catalysts. The TPR response recorded for the five supported Ni catalysts must represent a composite decomposition of the supported nitrate precursor with a subsequent (and possible concomitant) reduction of NiO to Ni^0 where any differences in the temperature requirements reflect differences in interfacial energies between nickel and each support. Ni/Al$_2$O$_3$ exhibits distinct behavior in that the reduction profile presents two distinguishable peaks, the second stage of reduction occurring during the final isothermal hold and must represent NiO reduction. TPR profiles for Ni/Al$_2$O$_3$ with one [64], two [65], and even four [51] reduction peaks have been reported in the literature. The higher temperature reduction suggests metal/support interaction that necessitates a higher reduction temperature: electron transfer from Al$_2$O$_3$ has been proposed elsewhere [66].

Pulse hydrogen chemisorption (under ambient conditions) measurements post TPR were used, assuming dissociative hydrogen adsorption, to determine specific metal surface areas; values are given in Table 1. Hydrogen uptake was higher on the supported catalysts when compared with bulk metal, as expected, where the support serves to disperse the metal, resulting in higher specific metal surface areas and increased gas uptake. Two catalysts (Pd/Al$_2$O$_3$ and Ni/AC) were subjected to comprehensive TEM analysis and representative images are given in Fig. 4, which also includes the particle size distribution histograms. The metal surface area obtained from the size distributions (based on total metal particle counts in excess of 800) agreed to within ± 8% with the values generated by hydrogen chemisorption.

TPD following H$_2$ chemisorption generated the profiles presented in Fig. 5 for Pd and Ni catalysts. Duplicate TPD measurements are included to demonstrate the degree of experimental reproducibility. TPD profiles for the supported catalysts are characterized by two broad peaks, a lower temperature peak with a T_{max} that spans the range 521–640 K (Pd catalysts) and 492–636 K (Ni catalysts) and a higher temperature peak with a T_{max} from 850 K that extends into the final isothermal hold (873 K). It is worth noting that Ni/Al$_2$O$_3$ presents three stages of TPD with an intermediate H$_2$ release (T_{max} = 785 K). Cesteros et al. [67] have also recorded three H$_2$ desorption peaks (T_{max} = ca. 410, 720, and 820 K) from Ni/Al$_2$O$_3$. TPD from unsupported Pd only exhibited a lower temperature H$_2$ release while there was no measurable H$_2$ desorption from bulk Ni; any H$_2$ desorbed from unsupported Ni was below detection limits (< 0.02
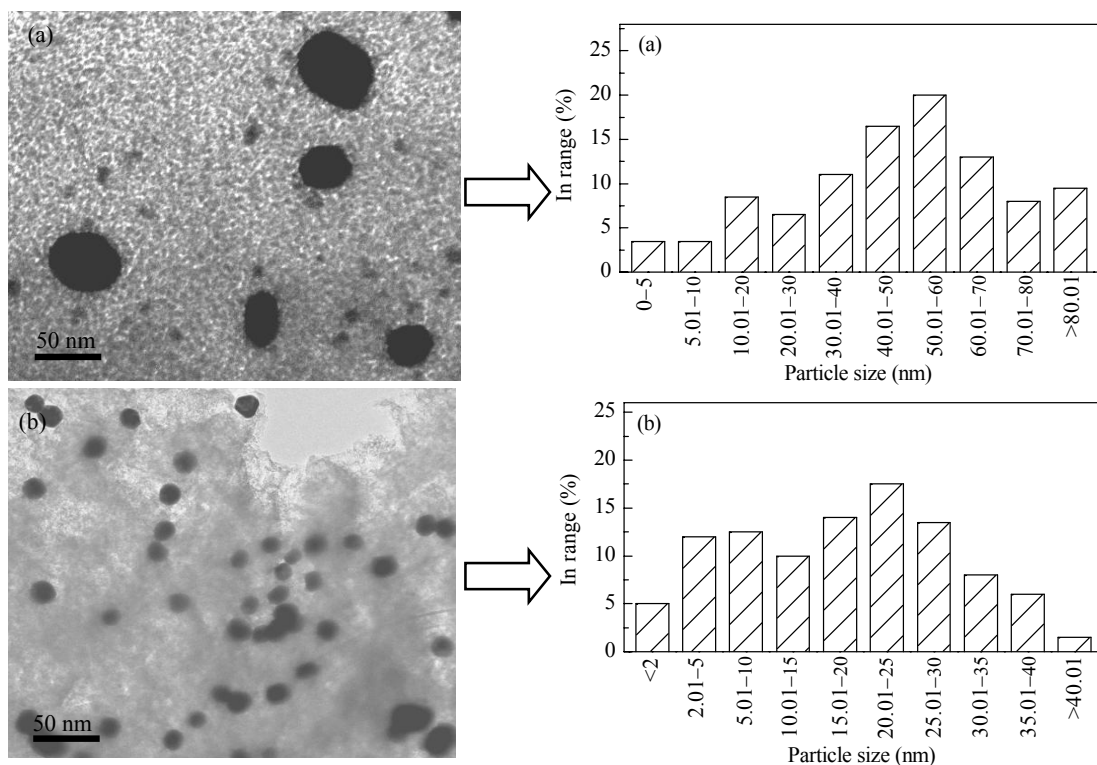
Fig. 4.   TEM images of Pd/Al$_2$O$_3$ (a) and Ni/AC (b) with associated particle size distribution histograms.

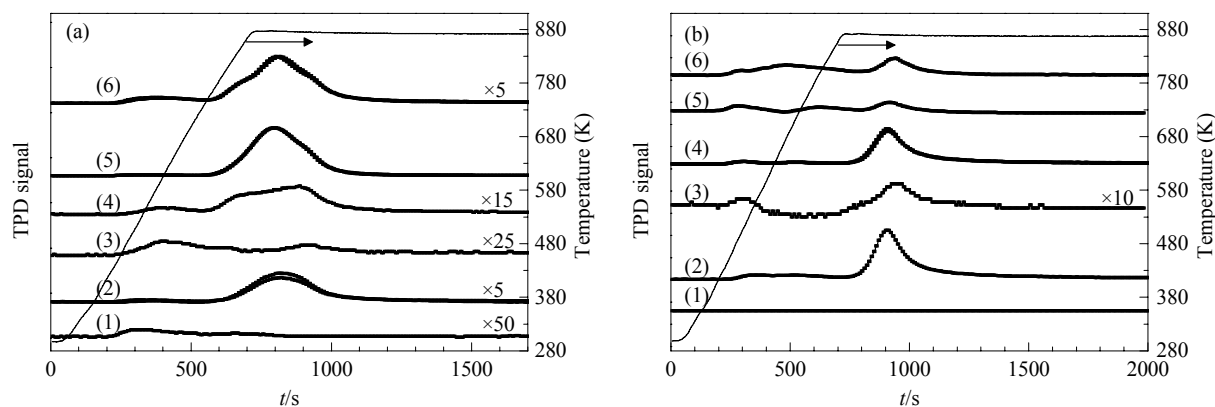**Fig. 5.**   H$_2$-TPD profiles of different catalyst samples. (a) Pd (1), Pd/AC (2), Pd/graphite (3), Pd/GNF (4), Pd/Al$_2$O$_3$ (5), Pd/SiO$_2$ (6); (b) Ni (1), Ni/AC (2), Ni/graphite (3), Ni/GNF (4), Ni/Al$_2$O$_3$ (5), Ni/SiO$_2$ (6).

cm^3/g). A direct comparison of the H$_2$-TPD profiles generated in this study with the limited reports in the literature is problematic given the differences in metal loading, support, catalyst preparation/activation and desorption procedure. Hydrogen TPD analysis is, nonetheless, a useful characterization technique to probe surface adsorbate/adsorbent (both metal and support) interactions and to evaluate (indirectly) metal/support effects. Indeed, it has been established that different H$_2$-TPD profiles are generated for the same metal (and similar loading) on different supports, e.g. 1 wt% Pd/C vs. Pd/Al$_2$O$_3$ [68] and 1.5 wt% Ni/SiO$_2$ vs. 2.2 wt% Ni/Y-zeolite [69]. In this study, the occurrence of the additional higher temperature desorption peak for the supported

catalysts can be attributed to the removal of spillover hydrogen from the support. This contention is consistent with the absence of a high temperature peak for the bulk metals. Moreover, the amount of H$_2$ released at $T < 785$ K (lower temperature peaks) matches that taken up in the chemisorption step (Table 1), which preceded TPD. In H$_2$-TPD analysis of supported metal catalysts, hydrogen spillover has been linked to desorption at $T > 503$ K, regardless of the metal or support [70–74]. The spillover phenomenon describes the migration of atomic hydrogen to the support after dissociation of molecular hydrogen on the metallic surface. Hydrogen spillover from metal to support has been reported in the literature for Pd [73–76] and Ni [69,71] on carbon [72–76],

Al₂O₃ [69,70] and SiO₂ [71] carriers. Ouchaib et al. [72] reported two H_2 desorption peaks from charcoal supported Pd at 373 and 673 K and attributed the higher temperature peak to spillover hydrogen. Dong et al. [74] concluded that hydrogen spillover takes place at 373 K on carbon supported Pd in order to account for H_2 uptake that exceeded the maximum Pd chemisorption capacity. Cheng et al. [75] recorded H_2 release from Pd/C during TPD that was higher than that predicted on the basis of the available surface Pd and attributed this to hydrogen spillover during the reduction step (at 473 K). It can be seen from the profiles in Fig. 5 that the amount of hydrogen spillover varies according to the support and, in the case of the Ni systems, increased in the order: Ni/graphite (0.1 cm³/g) < Ni/Al₂O₃ (0.4 cm³/g) < Ni/SiO₂ (0.7 cm³/g) < Ni/GNF (1.3 cm³/g) < Ni/AC (2.0 cm³/g). In the case of the Pd systems, Pd/Al₂O₃ generated the greatest amount of spillover hydrogen (12.1 cm³/g), Pd/AC and Pd/SiO₂, with quite different BET surface areas (see Table 1), delivered a similar high temperature hydrogen release ((2 ± 0.5) cm³/g), exceeding that recorded for Pd/GNF (0.7 cm³/g) and Pd/graphite (0.1 cm³/g). These results suggest that the support surface area is not the only factor that can govern the spillover phenomenon, which can be influenced by the nature and concentration of the initiating and acceptor sites and the degree of contact between the participating phases.

2.2 Catalytic activity for HDC of CB

Conversion of CB over unsupported and supported Ni generated benzene as the sole product, i.e. 100% selectivity with respect to HDC. In addition to benzene, cyclohexane (selectivity < 4%) was isolated in the product stream generated over supported/unsupported Pd, resulting from a further hydrogenation of benzene. Indeed, HDC was promoted to a far greater degree over the Pd systems and when the reaction was operated under identical conditions, the supported Pd catalysts delivered activities that were up to three orders of magnitude greater than those recorded for supported Ni, a result that is in agreement with an earlier study that compared the HDC action of Pd/SiO₂ with Ni/SiO₂ [76]. In the dechlorination of dichloromethane, Aristizabal et al. [77] found that the conversion over Pd/Al₂O₃ was almost double that obtained with Ni/Al₂O₃. Simagina et al. [23] reported a 95% hexachlorobenzene conversion over Pd/C under reaction conditions where Ni/C was inactive. Moreover, Gomez-Sainero et al. [78], in studying the dechlorination of carbon tetrachloride to chloroform, recorded the following activity sequence: Pd/C >> Pt/C > Rh/C > Ru/C > Ni/C. A distinction should be drawn between HDC and dehydrochlorination, the latter involving the internal elimination of HCl and is applicable to the

dechlorination of aliphatic chloro-compounds (including CFCs) [41], where an external H_2 source is not necessary but can serve to limit deactivation [42].

In order to generate comparable HDC rates for both Ni and Pd catalysts and to ensure some differentiation in catalytic response for the various supported systems, two sets of HDC operating conditions were employed in this study (see experimental section) and the resultant specific HDC rates (per metal surface area) are given in Table 2. It is noteworthy that bulk Pd outperformed the three carbon supported catalysts but was less active than the oxide based systems. In marked contrast, unsupported Ni exhibited no measurable activity under conditions where each supported Ni generated a significant HDC rate. In order to achieve a comparable fractional CB dechlorination to that obtained with supported Ni, an eightfold increase in the mass of unsupported Ni was required with an increase in the reaction temperature by 100 K (to 573 K).

Table 2 Specific CB HDC rates (r) delivered by Pd and Ni catalysts

Catalyst	r/(mol$_{Cl}$/(m²·h))
Pd	0.75
Pd/AC	0.50
Pd/graphite	0.15
Pd/GNF	0.28
Pd/Al₂O₃	3.00
Pd/SiO₂	2.20
Ni	—[a]
Ni/AC	0.011
Ni/graphite	0.059
Ni/GNF	0.041
Ni/Al₂O₃	0.010
Ni/SiO₂	0.005

[a] No measureable HDC activity.

While a consensus emerges from the literature that Pd is the most effective catalytic hydrodehalogenation agent, the precise source of this HDC efficiency has yet to be established. It is important to note that, as the decomposition of Pd hydride takes place where $T < 400$ K (see Fig. 2(a)) and HDC was performed at 423 K, any contribution due to Pd hydride can be discounted. The fact that the greater catalytic efficiency of Pd compared with Ni is not limited to HDC but also extends to hydrogenation reactions [79] suggests that H_2/surface interaction is a critical factor. Differences in the heat of adsorption of H_2 can be used to probe adsorption dynamics where Watson et al. [80] reported that H_2 adsorption energies on the (111) surface of Pd and Ni single crystals were similar but different from that for Pt(111). Chou and Vannice [81] reported a heat of H_2 adsorption on bulk Pd and Pd supported on SiO₂, SiO₂-Al₂O₃, Al₂O₃, and TiO₂ equal to (63 ± 4) kJ/mol, dependent on particle size but independent of support. Weatherbee et al. [82] observed a

support effect in the case of H_2 adsorption on Ni with a value of 90 kJ/mol for unsupported Ni, which is markedly lower than that recorded for Ni/Al_2O_3 (122 kJ/mol). The available database of experimental and calculated heats of H_2 adsorption on Pd and Ni is insufficient to serve as a reliable indicator of HDC activity. It is, however, significant that the diffusion coefficient for H_2 in Pd (ca. 10^{-11} m^2/s) [83,84] is three orders of magnitude greater than that for Ni (ca. 10^{-14} m^2/s) [85], which is at the same scale as the difference in HDC activity recorded in this study. Moreover, it has been demonstrated that H_2 diffusivity in Pd-Ni alloys decreases with increasing Ni content [86]. A search through the literature did not reveal an explicit link between H_2 diffusion coefficients for catalytically active transition metals and performance in H_2 mediated reactions. We tentatively attribute the more facile diffusion of H_2 in Pd systems relative to Ni as a possible source of higher HDC activity.

Specific HDC rates are plotted as a function of metal surface area (S) in Fig. 6 where (i) the higher specific activity associated with the Pd catalysts is immediately evident and (ii) Pd and Ni systems exhibit a different HDC dependence on metal area. The Ni catalysts show an increase in specific HDC rate with decreasing metal surface area, which appears to converge to a rate invariance where $S > 12$ m^2/g. HDC over bulk Pd and the three carbon supported Pd catalysts also increased with decreasing metal surface area but Pd/Al_2O_3 and Pd/SiO_2 deviated significantly from this trend by presenting appreciably higher activities. Previous studies have shown that dehalogenation rates are enhanced at lower metal dispersion (or larger particle sizes) for both Ni [19,34]
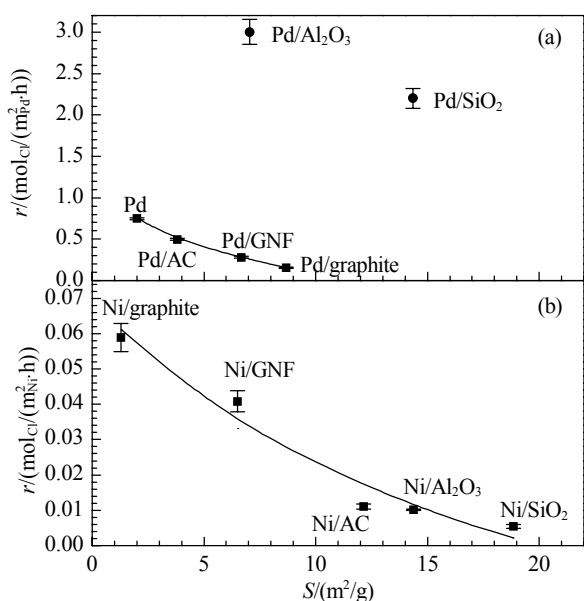
and Pd [87] catalysts, which was taken as evidence for structure sensitivity. In a number of dechlorination studies [29,31,34,35] that have involved unsupported metal catalysts, the dechlorination action of related supported metals was not considered. The studies that have compared dehalogenation performance of bulk and supported metals deal with gas phase CFC [30,33,88] and liquid phase CB [28] reactions. Rioux et al. [30] showed that CFC turnover rates recorded for Pd/C were equal to or four times greater than that of Pd black. It should, however, be noted that CFC transformation involves a dehydrohalogenation and structure/activity relationships can differ from that which holds for catalytic HDC. Wu and Xu [28] recorded higher CB conversions over Raney Ni relative to Ni/Al_2O_3 and Ni/SiO_2 but they did not provide characterization data that allow a direct comparison of specific activities. Morato et al. [33] have reported higher CFC-12 and HCFC-22 turnover frequencies for bulk Ni relative to Ni supported on activated carbon or graphite. The higher activity delivered by unsupported Ni was attributed to particle size and morphology effects where octahedral particles were proposed to possess greater dehalogenation efficiency. In contrast, we did not observe any CB HDC activity for unsupported (cubic) Ni under conditions where supported Ni catalysts presented significant activities.

The range of specific HDC rates recorded in Fig. 6 for supported metals suggests a catalyst support effect, especially when considering the higher activities delivered by Al_2O_3 and SiO_2 supported Pd. The supported Pd systems exhibited a twenty-fold difference in specific rate between the least (Pd/graphite) and most (Pd/Al_2O_3) active catalysts while the values delivered by supported Ni differ by a factor of twelve when comparing the least (Ni/SiO_2) and most (Ni/graphite) active catalysts. Although an explicit link between catalyst support and HDC performance has yet to be established, there are a number of pertinent published studies that should be flagged. Benitez et al. [8] compared (liquid phase) CB HDC behaviour of three supported Pd catalysts and recorded the following activity sequence: Pd/SiO_2 > Pd/Al_2O_3 > Pd/C. On the other hand, in gas phase operation, Prati et al. [7] reported decreasing CB HDC activity in the order: Pd/C > Pd/Vycor (porous glass) > Pd/Al_2O_3 >> Pd/AlF_3. Wu and Xu [28] observed an increasing (liquid phase) CB HDC activity sequence, i.e. Ni/AC >> Ni/Al_2O_3 > Ni/SiO_2, that was attributed to the surface chemistry of the supports but the authors did not develop this correlation further. It is important to stress the divergence in the operation of batch liquid phase HDC reactions from our gas phase continuous flow system, notably with respect to temperature, contact time, and reactant feed concentration. Moreover, surface hydrophobicity/hydrophilicity and the involvement of a solvent can have a dramatic influence on

Fig. 6. Specific CB HDC rate (r) as a function of metal surface area (S) for reaction over the Pd systems (a) and the Ni systems (b). The error bars represent experimental reproducibility.

liquid phase HDC where solution pH is a paramount factor [88–90]. Given the number of (interrelated) factors that can have a bearing on catalytic efficiency, it is difficult to pinpoint one catalyst property that determines HDC performance. However, it is clear from our results that metal-support interaction is a contributory factor, impacting on TPR characteristics, ultimate metal surface area, H_2 uptake/release and the consequent HDC response. There is some evidence in the literature [91,92] for the involvement of spillover hydrogen in catalytic HDC. It is significant that the highest HDC rates were obtained with those catalysts (notably Pd/Al_2O_3) that exhibited high spillover content. This suggests a surface synergistic effect where the occurrence of spillover contributes to enhanced HDC performance. However, it should be noted that we have only considered the interaction of one of the reactants (H_2) with our family of catalysts and the dynamics of CB/surface (both metal and support) interaction can have a major bearing. A concerted effort to probe the nature of CB activation leading to C-Cl bond hydrogenolysis will form the basis of a future study.

3　Conclusions

Bulk and supported (on AC, graphite, GNF, Al_2O_3, and SiO_2) Pd and Ni catalyst systems demonstrated quite distinct catalytic behaviour in gas phase CB HDC. While conversion of CB was 100% selective with respect to HDC over Ni, cyclohexane (selectivity < 4%) was also generated over supported/unsupported Pd. Under the same operating conditions, supported Pd catalysts delivered specific HDC rates that were up to three orders of magnitude greater than that recorded for supported Ni. HDC performance of bulk Pd exceeded that of Pd on the three carbon supports while unsupported Ni was inactive under conditions where supported Ni exhibited significant HDC activity. We propose that the higher activity delivered by Pd relative to Ni is associated with a more facile diffusion of H_2 in Pd. A support effect is evident from the range of surface areas exhibited by the supported metals and the divergence in the TPR and H_2 TPD response. Specific HDC rates over both supported Pd and Ni systems increased with decreasing specific metal area. Pd/Al_2O_3 and Pd/SiO_2 deviate from a common trend line and delivered significantly higher HDC activities, a response that we ascribe to a contribution due to spillover hydrogen.

References

1　Goldberg E D. *Sci Total Environ*, 1991, **100**: 17
2　Thornton J. Pandora's Poison: Chlorine Health and a New Environmental Strategy. Cambridge: MIT Press, 2000
3　Urbano F J, Marinas J M. *J Mol Catal A*, 2001, **173**: 329
4　Keane M A. *J Chem Technol Biotechnol*, 2005, **80**: 1211
5　Brinkman D W, Dickson J R, Wilkinson D. *Environ Sci Technol*, 1995, **29**: 87
6　Shao Y, Xu Z, Wan H, Chen H, Liu F, Li L, Zheng S. *J Hazard Mater*, 2010, **179**: 135
7　Prati L, Rossi M. *Appl Catal B*, 1999, **23**: 135
8　Benitez J L, Del Angel G. *React Kinet Catal Lett*, 2000, **70**: 67
9　Yakovlev V A, Terskikh V V, Simagina V I, Likholobov V A. *J Mol Catal A*, 2000, **153**: 231
10　Babu N S, Lingaiah N, Pasha N, Kumar J V, Prasad P S S. *Catal Today*, 2009, **141**: 120
11　Babu N S, Lingaiah N, Gopinath R, Reddy P S S, Prasad P S S. *J Phys Chem C*, 2007, **111**: 6447
12　Lingaiah N, Prasad P S S, Rao P K, Berry F J, Smart L E. *Catal Commun*, 2002, **3**: 391
13　Jujjuri S, Ding E, Shore S G, Keane M A. *Appl Organomet Chem*, 2003, **17**: 493
14　Gopinath R, Rao K N, Prasad P S S, Madhavendra S S, Narayanan S, Vivekanandan G. *J Mol Catal A*, 2002, **181**: 215
15　Lingaiah N, Prasad P S S, Rao P K, Smart L E, Berry F J. *Appl Catal A*, 2001, **213**: 189
16　Ukisu Y, Miyadera T. *J Mol Catal A*, 1997, **125**: 135
17　Keane M A. In: Keane M A Ed. Interfacial Applications in Environmental Engineering. New York: Marcel Dekker, 2002. 231
18　Menini C, Park C, Shin E J, Tavoularis G, Keane M A. *Catal Today*, 2000, **62**: 355
19　Keane M A, Park C, Menini C. *Catal Lett*, 2003, **88**: 89
20　Keane M A, Larsson R. *J Mol Catal A*, 2007, **268**: 87
21　Keane M A, Larsson R. *Catal Commun*, 2008, **9**: 333
22　Chen J X, Sun L M, Wang R J, Zhang J Y. *Catal Lett*, 2009, **133**: 346
23　Simagina V, Likholobov V, Bergeret G, Gimenez M T, Renouprez A. *Appl Catal B*, 2003, **40**: 293
24　Chen J X, Zhou S J, Ci D H, Wang R J, Zhang J Y. *Ind Eng Chem Res*, 2009, **48**: 3812
25　Keane M A, Tavoularis G. *React Kinet Catal Lett*, 2003, **78**: 11
26　Yoneda T, Takido T, Konuma K. *Appl Catal B*, 2008, **84**: 667
27　Park C, Keane M A. *ChemPhysChem*, 2001, **2**: 733
28　Wu W, Xu J. *Catal Commun*, 2004, **5**: 591
29　Ribeiro F H, Gerken C A, Rupprechter G, Somorjai G A, Kellner C S, Coulston G W, Manzer L E, Abrams L. *J Catal*, 1998, **176**: 352
30　Rioux R M, Thompson C D, Chen N, Ribeiro F H. *Catal Today*, 2000, **62**: 269
31　Ramos A L D, Schmal M, Aranda D A G, Somorjai G A. *J Catal*, 2000, **192**: 423
32　Zinovyev S, Perosa A, Yufit S, Tundo P. *J Catal*, 2002, **211**: 347
33　Morato A, Alonso C, Medina F, Salagre P, Sueiras J E, Terrado R, Giralt A. *Appl Catal B*, 1999, **23**: 175
34　Estelle J, Ruz J, Cesteros Y, Fernandez R, Salagre P, Medina F, Sueiras J-E. *J Chem Soc, Faraday Trans*, 1996, **92**: 2811

35 Zhang W X, Wang C B, Lien H L. *Catal Today*, 1998, **40**: 387

36 Bonarowska M, Burda B, Juszczyk W, Pielaszek J, Kowalczyk Z, Karpinski Z. *Appl Catal B*, 2001, **35**: 13

37 Amorim C, Yuan G, Patterson P M, Keane M A. *J Catal*, 2005, **234**: 268

38 Park C, Keane M A. *Catal Commun*, 2001, **2**: 171

39 Benson J E, Hwang H S, Boudart M. *J Catal*, 1973, **30**: 146

40 JCPDS-ICDD, PCPDFWIN, Version 2.2, June 2001

41 Tavoularis G, Keane M A. *J Mol Catal A*, 1999, **142**: 187

42 Tavoularis G, Keane M A. *Appl Catal A*, 1999, **182**: 309

43 Park C, Keane M A. *J Colloid Interf Sci*, 2003, **266**: 183

44 Serp P, Corrias M, Kalck P. *Appl Catal A*, 2003, **253**: 337

45 Wei H W, Leou K C, Wei M T, Lin Y Y, Tsai C H. *J Appl Phys*, 2005, **98**: 044313

46 Wang H J, Zhao F Y, Fujita S I, Arai M. *Catal Commun*, 2008, **9**: 362

47 Ledoux M J, Pham-Huu C. *Catal Today*, 2005, **102-103**: 2

48 Coelho N M D, Furtado J L B, Pham-Huu C, Vieira R. *Mater Res*, 2008, **11**: 353

49 Planeix J M, Coustel N, Coq B, Brotons V, Kumbhar P S, Dutartre R, Geneste P, Bernier P, Ajayan P M. *J Am Chem Soc*, 1994, **116**: 7935

50 Dai H, Bell A T, Iglesia E. *J Catal*, 2004, **221**: 491

51 Hu C-W, Yao J, Yang H-Q, Chen Y, Tian A-M. *J Catal*, 1997, **166**: 1

52 Nag N K. *J Phys Chem B*, 2001, **105**: 5945

53 Baranowski B, Wisniewski R. *Bull Acad Polon Sci Ser Sci Chim*, 1966, **14**: 273

54 Gomez-Sainero L M, Seoane X L, Fierro J L G, Arcoya A. *J Catal*, 2002, **209**: 279

55 Wang C B, Lin H K, Ho C M. *J Mol Catal A*, 2002, **180**: 285

56 Tonetto G M, Damiani D E. *J Mol Catal A*, 2003, **202**: 289

57 Garcia G, Vargas J R, Valenzuela M A, Rebollar M, Acosta D. *Mater Res Soc Symp Proc*, 1999, **549**: 237

58 Pinna F, Menegazzo F, Signoretto M, Canton P, Fagherazzi G, Pernicone N. *Appl Catal A*, 2001, **219**: 195

59 Murthy K V, Patterson P M, Keane M A. *J Mol Catal A*, 2005, **225**: 149

60 Mizushima T, Nishida K, Ohkita H, Kakuta N. *Bull Chem Soc Jpn*, 2002, **75**: 2283

61 Diaz A, Acosta D R, Odriozala J A, Montes M. *J Phys Chem B*, 1997, **101**: 1782

62 Rynkowski J, Rajski D, Szyszka I, Grzechowiak J R. *Catal Today*, 2004, **90**: 159

63 González-Marcos M P, Gutiérrez-Ortiz J I, González-Ortiz de Elguea C, González-Velasco J R. *J Mol Catal A*, 1997, **120**: 185

64 Roh H-S, Jun K-W, Dong W-S, Chang J-S, Park S-E, Joe Y-I. *J Mol Catal A*, 2002, **181**: 137

65 Xu G, Shi K, Gao Y, Xu H, Wei Y. *J Mol Catal A*, 1999, **147**: 47

66 Dropsch H, Baerns M. *Appl Catal A*, 1997, **158**: 163

67 Cesteros Y, Salagre P, Medina F, Sueiras J E. *Appl Catal B*, 1999, **22**: 135

68 Yuan G, Keane M A. *Catal Today*, 2003, **88**: 27

69 Shin E J, Keane M A. *Ind Eng Chem Res*, 2000, **39**: 883

70 Benseradj F, Sadi F, Chater M. *Appl Catal A*, 2002, **228**: 135

71 Shin E J, Spiller A, Tavoularis G, Keane M A. *Phys Chem Chem Phys*, 1999, **1**: 3173

72 Ouchaib T, Moraweck B, Massardier J, Renouprez A. *Catal Today*, 1990, **7**: 191

73 Ramos A L D, Aranda D A G, Schmal M. *Stud Surf Sci Catal*, 2001, **138**: 291

74 Dong J S, Park T J, Ihm S K. *Carbon*, 1993, **31**: 427

75 Cheng Z X, Yuan S B, Fan J W, Zhu Q M, Zhen M S. *Stud Surf Sci Catal*, 1997, **112**: 261

76 Keane M A. *Appl Catal A*, 2004, **271**: 109

77 Aristizabal B, Gonzalez C A, Barrio I, Montes M, de Correa C M. *J Mol Catal A*, 2004, **222**: 189

78 Gomez-Sainero L M, Cortes A, Seoane X L, Arcoya A. *Ind Eng Chem Res*, 2000, **39**: 2849

79 Cárdenas-Lizana F, Gómez-Quero S, Keane M A. *Appl Catal A*, 2008, **334**: 199

80 Watson G W, Wells R P K, Willock D J, Hutchings G J. *Chem Commun*, 2000: 705

81 Chou P, Vannice M A. *J Catal*, 1987, **104**: 1

82 Weatherbee G D, Bartholomew C H. *J Catal*, 1984, **87**: 55

83 Takano N, Murakami Y, Terasaki F. *Scripta Metall Mater*, 1995, **32**: 401

84 Ishikawa T, McLellan R B. *Acta Metall*, 1985, **33**: 1979

85 Ansari N, Balasubramaniam R. *Mater Sci Eng A*, 2000, **293**: 292

86 Dos Santos D S. *Defect Diffus Forum*, 2002, **203-2**: 219

87 Aramendia M A, Borau V, Garcia I M, Jimenez C, Marinas J M, Urbano F J. *Appl Catal B*, 1999, **20**: 101

88 Yuan G, Keane M A. *J Catal*, 2004, **225**: 510

89 Yuan G, Keane M A. *Appl Catal B*, 2004, **52**: 301

90 Gómez-Quero S, Cárdenas-Lizana F, Keane M A. *AICHE J*, 2010, **56**: 756

91 Keane M A, Murzin D Y. *Chem Eng Sci*, 2001, **56**: 3185

92 Liu X G, Chen J X, Zhang J Y. *Ind Eng Chem Res*, 2008, **47**: 5362